A multiscale reduced-order-model strategy for transient thermoelasticity with variable microstructure

Mainak Bhattacharyya, David Dureisseix

A multi-scale reduced-order-model strategy for transient thermo-elasticity with variable micro-structure

Mainak Bhattacharyya[1] and David Dureisseix[2]

[1] Laboratoire Roberval, Université de Technologie de Compiègne, Centre de recherche Royallieu, F-60203 Compiègne Cedex, France
[2] Univ Lyon, INSA-Lyon, CNRS UMR5259, LaMCoS, F-69621, France

Abstract

This article deals with thermo-elastic computation of heterogeneous structures containing quasi-periodic micro-structures having variable properties (geometric and/or material) using reduced order modelling. Such heterogeneous structure is extremely expensive to simulate using classical finite element methods, as the level of discretisation required to capture the micro-structural effects, is too fine. Based on the asymptotic homogenisation theory, the multi-scale technique explores the micro-macro behaviour for thermo-elasticity. Considering each integration point of the macro-structure consists of an underlying locally-periodic micro-structure, the overall problem is basically separated into a homogeneous problem defined over the macro-structure and a heterogeneous problem defined over each micro-structure. Even though the usage of multi-scale strategy helps in the reduction of numerical expense, it still deals with a full order finite element solution for the macro-problem and each micro-problem. Using a 2-fold reduced order modelling further accentuates the cost reduction and provides a robust solution in a reduced space: (i) as an offline pre-computation stage for the micro-structural problem, and (ii) as an online process that can embed adaptivity for the macroscopic problem.

This is a preprint of an article published in its final form as: ***

Keywords. multi-scale, asymptotic homogenisation, variable micro-structures, thermo-elasticity, surrogate model

1 Introduction

Heterogeneous structures are typically common in the engineering world and are used in many applications. Typical examples can be composites, alloys, porous media and so on. This kind of structures generally consists of more than one phase, and the heterogeneity is exhibited at a microscopic scale. Obviously the overall physical behaviour depends on the size, shape, material properties and distribution of the microscopic constituents. A classical finite element (FE) simulation for such cases is extremely expensive as the level of discretisation needed to substantiate the underlying micro-heterogeneities will be too fine for real engineering structures. To circumvent this difficulty multi-scale models have been developed over the years.

The idea herein is to propose a multi-scale strategy for thermo-elasticity for variable micro-structures. We target a transient classical elliptic thermal problem while while quasi-static mechanical behaviour is concerned. This model is indeed related to characteristic times of the loading: smaller than the thermal diffusion one (but larger than the so-called thermal wave one), larger than the mechanical wave equation one. The main philosophy behind classical multi-scale methods is the assumption of existence of periodic micro-structures or at least locally periodic micro-structures at a length scale which is small compared to the macro-scale. The macroscopic structure is assumed to be homogeneous and the homogeneity is quantified through the simulation of micro-structures. The macroscopic structure can be simulated using classical finite element method and existence of micro-structures (can also be termed as unit cells) are assumed at macroscopic integration points. The micro-structural unit cells contain the heterogeneities, i.e. they are made of more than one material. The micro-problems can also be simulated using classical finite element method, and the number of micro-structural simulations is equal to the number of macroscopic integration points. There are few ways in which the aforementioned philosophy can be executed [17]. One of them is the FE^2 approach [40, 21, 20, 41, 28] where no explicit constitutive relations are needed at the macroscopic scale and each integration point of the macroscopic structure constitutes of an underlying micro-structure. Knowing the mechanical state at the micro-scale, the macroscopic state variables at each integration point can be calculated through homogenisation [9, 10, 29]. Some of the recent developments in the field of FE^2 methods can be seen in many noteworthy works [15, 22, 16]. There

exist another type of multi-scale method, which is based on the asymptotic expansion of the state variables with respect to a scaling factor [1, 38]. This type of expansion thereby can be utilised in the governing equations which can then be separated into microscopic and macroscopic problems. The asymptotic homogenisation can provide effective overall structural response including their local microscopic counterparts. Initially this type of methods were used to solve elastic problems especially for composites [12, 7], for Cosserat media [14]. A generalisation of the mathematical homogenisation based on eigenstrains for heterogeneous structures was done for elasto-plasticity [11], for non-local brittle damage [13]. Some other recent application was to find the effect of damage amplification due to micro-crack interaction [25], to simulate thermoelectric composites [44]. With respect to thermal problems, multi-scale methods has been used for transient heat conduction [27, 33, 19, 26] and for conduction-radiation problems [18]. For coupled thermo-mechanical problems, there has been works on random particulate composites [47] and on FE^2 methods [34].

The aim of multi-scale methods is to reduce the numerical expense drastically by reducing the overall micro-structural computation to only micro-structural cells behind the macroscopic integration points. However, this still requires full order FE calculations both at macro level and at the unit cell level, which can render the complete process significantly expensive. This is the basic motivation behind the usage of reduced order models, which gives low fidelity approximations of high fidelity model, and thereby reducing the CPU cost. The reduced order strategy used herein is Proper Orthogonal Decomposition (POD) which is to compute certain full-order problems (called the training stage) in order to extract relevant information which can then be used to calculate similar problems more efficiently. The usage of POD in the field of mechanics deals with the creation of POD basis, from the snapshots obtained from the solution of the training stage, and then to use this basis to solve the intended problem in a reduced space [37]. Also known as Principal Component Analysis (PCA), Karhunen–Loève Expansion (KLE) and Singular Value Decomposition (SVD) [4], POD provides an optimally ordered set of basis functions in a least square sense for the full-order solution. A reduced order model or a surrogate model can then be generated by truncating the optimal basis [35, 23]. On the paradigm of multi-scale methods, POD and its variants have been used for non-linear heat conduction [31], for multi-scale fracture mechanics [32], for hyper-elastic materials at finite strains [45], for damage analysis [3, 2] and such others.

As a novelty, this article exemplifies the interest in terms of computational cost reduction of using the synergy between parametric homogenisation and POD at two scales: (i) at micro-scale, homogenised quantities are the quantities of interest (QoI) and the POD is used to deal with the parametric aspect; (ii) an independent POD at macro-scale only is used to build a reduced basis onto which the macroscopic solution is projected, the underlying micro-scale POD is used as a reduced order model to provide the QoI as function of the parametric macro fields to further enhance numerical frugality. This type of strategy reduces the simulation cost extremely and can also be used effectively for variable micro-structures. Variations in this article is restricted to micro-structural material properties and fibre diameter altering with respect to macroscopic parameter fields.

The article begins with the definition of the problem in Section 2 with all the governing equations. The multi-scale strategy based on asymptotic theory along with scale separations are discussed in Section 3. Thereafter, the solution strategy introducing linear operators, extension for variable micro-structures and the reduced order strategy is detailed in Section 4. Finally the strategy is exemplified in Section 5 with conclusion and perspectives in Section 6.

2 Problem definition

Consider a heterogeneous structure in the domain Ω, fig. 1(a). The mechanical boundary $\partial\Omega$ of the domain is split into $\partial\Omega_{m1}$ where a prescribed displacement $\underline{U}_d$ is specified, and the complementary boundary $\partial\Omega_{m2}$ submitted to a surface traction $\underline{F}_d$. The same boundary $\partial\Omega$ can also be split into $\partial\Omega_{t1}$ with an applied temperature θ_d and $\partial\Omega_{t1}$ where external heat flux density q_s is applied. The heterogeneous media is composed of microscopic locally periodic representative volume elements (RVEs) containing at least two different materials.

Considering the thermal problem as depicted in, Fourier's law of heat conduction reads

$$\underline{q} = -k\nabla\theta \quad \text{in } \Omega, \tag{1}$$

where $\underline{q}$ is the vector of heat flux density, θ is the temperature field and k is the thermal conductivity. The operator ∇ represents the classical gradient operator with respect to the spatial coordinates. The heat flow equation at a given time t, in the absence of internal heat source reads

$$-\nabla \cdot \underline{q} = \rho c\dot{\theta} \quad \text{in } \Omega, \tag{2}$$

where ρ is the mass density of the material, and c is the specific heat capacity. The operator $\nabla\cdot$ represents the classical divergence operator with respect to the spatial coordinates. For simplicity, it is considered that there is no adiabatic overheating, i.e. there is no internal heat generation due to mechanical dissipation or any other sources, i.e. the thermo-mechanical coupling is one way.

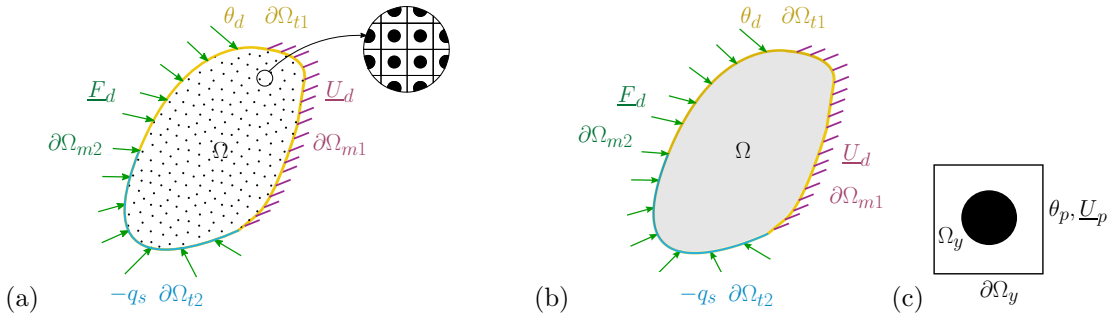

Figure 1: (a) Heterogeneous continua with periodic micro-structure, (b) equivalent macroscopic structure, and (c) microscopic unit cell

The boundary conditions of the structure can be of Dirichlet type i.e.

$$\theta = \theta_d \quad \text{on } \partial\Omega_{t1}. \tag{3}$$

The Neumann type boundary condition on the complementary surface can be written as

$$\underline{q} \cdot \underline{n} = -q_s \quad \text{on } \partial\Omega_{t2}, \tag{4}$$

where $\underline{n}$ is the unit vector normal to the surface $\partial\Omega_{t2}$. The initial condition is given by

$$\theta(t=0) = \theta^{\text{in}} \quad \text{in } \Omega, \tag{5}$$

where θ^{in} is the initial temperature field, taken as zero in all of the following, for simplicity.

Considering the mechanical part of the problem, the equilibrium of the structure is then given by

$$\nabla \cdot \sigma = 0 \quad \text{in } \Omega, \tag{6}$$

with the boundary conditions,

$$\sigma \cdot \underline{n} = \underline{F}_d \quad \text{on } \partial\Omega_{m2}, \tag{7}$$

$$\underline{u} = \underline{U}_d \quad \text{on } \partial\Omega_{m1}. \tag{8}$$

The quantity σ is the Cauchy stress tensor, $\underline{n}$ being the unit normal at each point on the surface $\partial\Omega_{m2}$, and $\underline{u}$ is the displacement field. The strain displacement relationship for infinitesimal strain tensor ε can be written as

$$\varepsilon = \nabla^s \underline{u} \quad \text{in } \Omega, \tag{9}$$

with $\nabla^s \circ = 1/2 \left[\nabla \circ + (\nabla \circ)^T\right]$ as the symmetric part of the gradient.

Apart from such admissibility conditions, the state of the structure at each material point is also described by thermo-elastic constitutive equation which is local in space:

$$\sigma = \mathbf{C}\left(\varepsilon - \alpha\theta\delta\right) \quad \text{in } \Omega, \tag{10}$$

where α is the coefficient of thermal expansion, δ is the identity tensor and $\mathbf{C}$ is the Hooke elasticity tensor.

It must be noted that the thermo-mechanical coupling is one way and any adiabatic overheating and any internal heat generations are neglected. The mechanical loads essentially do not influence the thermal problem. In such case, the thermal problem is sometimes entirely solved in one stage, then the mechanical one only at specific time steps. Nevertheless, for some verification design cases, the mechanical stress is indeed required during transient steps for thermal loading that leads to complex stress redistributions. Therefore, in the present study, the mechanical problem during all time evolution is solved together with the thermal problem.

3 Separation of scales

The periodic homogenisation based on asymptotic expansion is briefly recalled herein for completion [1, 38], and applied to the coupled thermo-mechanical problem under concern. Two spatial coordinates are used, namely the slow one $\underline{x}$, describing the evolutions at macro scale, and the fast one $\underline{y}$, describing the evolutions at micro scale, once a scaling factor ξ is used as:

$$\underline{y} = \frac{\underline{x}}{\xi}. \tag{11}$$

This factor (assumed to be small to ensure the scale separation) is defined as the ratio of the unit cell characteristic length and the overall structure length. Such a scale separation transforms the macroscopic structural domain into an equivalent quasi-homogeneous continua, see fig. 1(b), and defines a heterogeneous RVE (unit cell) over which the averaging is performed, see fig. 1(c). It is also assumed that the unit cells are locally periodic or y-periodic. The various fields in the problem now depends spatially on these two coordinates and are periodic with respect to the $\underline{y}$ one. This implies that s

$$\langle \nabla_y \cdot \chi \rangle_y = 0, \quad \langle \nabla_y \underline{\kappa} \rangle_y = 0, \quad \text{and} \quad \langle \nabla_y \vartheta \rangle_y = 0, \tag{12}$$

for any tensor field $\chi(\underline{x}, \underline{y})$, any vector field $\underline{\kappa}(\underline{x}, \underline{y})$, and any scalar field $\vartheta(\underline{x}, \underline{y})$ when derivation is made with respect to the $\underline{y}$ coordinates, which is depicted with a y subscript. The averaging operator $\langle \circ \rangle_y$ is defined as

$$\langle \circ \rangle_y (\underline{x}) = \frac{1}{V_y} \int_{\Omega_y} \circ(\underline{x}, \underline{y}) \, \mathrm{d}V, \tag{13}$$

where V_y is the volume of the unit cell.

The domain of the macroscopic problem is Ω with the boundaries being $\partial\Omega_{t1}, \partial\Omega_{t2}, \partial\Omega_{m1}, \partial\Omega_{m2}$ where the corresponding Dirichlet and/or Neumann boundary conditions are applied. The domain of the microscopic unit cell is Ω_y with boundary $\partial\Omega_y$ where periodic boundary conditions are prescribed.

The primary unknowns of the problem, herein the temperature and the displacement fields, are then developed asymptotically with respect to the scale ratio, as

$$\theta(\underline{x}, \underline{y}) = \theta_0(\underline{x}, \underline{y}) + \xi\theta_1(\underline{x}, \underline{y}) + \xi^2\theta_2(\underline{x}, \underline{y}) + \cdots \tag{14}$$

$$\underline{u}(\underline{x}, \underline{y}) = \underline{u}_0(\underline{x}, \underline{y}) + \xi\underline{u}_1(\underline{x}, \underline{y}) + \xi^2\underline{u}_2(\underline{x}, \underline{y}) + \cdots \tag{15}$$

all functions being periodic with respect to the $\underline{y}$ coordinate.

3.1 Thermal problem

According to eq. (11), the gradient of the temperature field can be written as

$$\nabla\theta = \nabla_x\theta \left(\underline{x}, \underline{y}\right) + \frac{1}{\xi}\nabla_y\theta \ \left(\underline{x}, \underline{y}\right), \tag{16}$$

where the subscripts x and y represent derivatives with respect to macro and micro scales, respectively. Using eq. (16) and (14), the thermal problem of eq. (1) and (2) can be written as

$$\begin{aligned} &\frac{1}{\xi^2}\nabla_y \cdot (k\nabla_y\theta_0) + \frac{1}{\xi}\left[\nabla_x \cdot (k\nabla_y\theta_0) + \nabla_y \cdot (k\nabla_x\theta_0) + \nabla_y \cdot (k\nabla_y\theta_1)\right] \\ &\quad + \left[\nabla_x \cdot (k\nabla_x\theta_0) + \nabla_x \cdot (k\nabla_y\theta_1) + \nabla_y \cdot (k\nabla_x\theta_1) + \nabla_y \cdot (k\nabla_y\theta_2)\right] + \cdots = \rho c\dot{\theta}_0 + \xi\rho c\dot{\theta}_1 + \cdots . \end{aligned} \tag{17}$$

The next step hereafter is to generate different orders of boundary value problem by equating terms with equal powers of ξ.

-2 order problem. Equating terms containing ξ^{-2} leads to

$$\nabla_y \cdot (k\nabla_y\theta_0) = 0. \tag{18}$$

This immediately provides θ_0 to be independent of $\underline{y}$, which can be seen as the macroscopic temperature and for the sake of clarity will be denoted in the following as $\theta_0 = \theta_M(\underline{x})$. Its gradient with respect to $\underline{x}$ being the macroscopic temperature gradient $\underline{z}_M(\underline{x}) = \nabla_x\theta_M$.

-1 order problem. Equating terms containing ξ^{-1}, using eq. (18), leads to

$$\nabla_y \cdot (k\nabla_y\theta_1) = -\nabla_y \cdot (k\underline{z}_M) . \tag{19}$$

This is the steady-state microscopic problem , whose unknown is $\theta_1(\underline{x}, \underline{y})$, parametrised by the macroscopic gradient $\underline{z}_M(\underline{x}, \underline{y})$, defined in the unit cell domain once the y-periodicity of θ_1 is added. The total heat flux vector, once the approximation is truncated to the level 1 in the expansion, becomes

$$\underline{q}(\underline{x}, \underline{y}) = -k\left(\underline{z}_M + \nabla_y\theta_1\right) \quad \text{in } \Omega_y. \tag{20}$$

0 **order problem.** Equating terms containing ξ^0 leads to the transient thermal problem

$$\nabla_x \cdot (k\underline{z}_M) + \nabla_x \cdot (k\nabla_y \theta_1) + \nabla_y \cdot (k\nabla_x \theta_1) + \nabla_y \cdot (k\nabla_y \theta_2) = \rho c \dot{\theta}_M \tag{21}$$

Now applying the averaging operator, eq. (21) transforms into

$$\nabla_x \cdot \left(\langle k \rangle_y \nabla_x \theta_M \right) + \nabla_x \cdot \langle k\nabla_y \theta_1 \rangle_y = \langle \rho c \rangle_y \dot{\theta}_M \tag{22}$$

Adding the initial and boundary conditions, this leads to the macroscopic problem defined in Ω as

$$\begin{aligned} \nabla_x \cdot \left(\langle k \rangle_y \nabla_x \theta_M + \langle k\nabla_y \theta_1 \rangle_y \right) = \langle \rho c \rangle_y \dot{\theta}_M \quad &\text{in } \Omega, \\ \theta_M = \theta_d \quad &\text{on } \partial\Omega_{t1}, \\ \underline{q}_M \cdot \underline{n} = -q_s \quad &\text{on } \partial\Omega_{t2}, \\ \theta_M(t=0) = 0 \quad &\text{in } \Omega, \end{aligned} \tag{23}$$

where the macroscopic heat flux vector is given by

$$\underline{q}_M(\underline{x}) = \langle \underline{q} \rangle_y = -\langle k \rangle_y \nabla_x \theta_M - \langle k\nabla_y \theta_1 \rangle_y \quad \text{in } \Omega. \tag{24}$$

One way of solving the multi-scale problem is to perform fixed point iteration between the BVPs of the two-scales. However that would be computationally non-frugal, so to avoid the iterations, an alternative strategy will be required. The full solution for the temperature and the heat flux density can then be recovered as $\theta(\underline{x}, \underline{y}) = \theta_M(\underline{x}) + \xi\theta_1(\underline{x}, \underline{y})$ and (20).

3.2 Mechanical problem

According to eq. (11), the mechanical problem can be obtained as

$$\nabla \cdot \sigma = \nabla_x \cdot \sigma \left(\underline{x}, \underline{y} \right) + \frac{1}{\xi} \nabla_y \cdot \sigma \left(\underline{x}, \underline{y} \right), \tag{25}$$

$$\varepsilon = \nabla_x^s \underline{u} \left(\underline{x}, \underline{y} \right) + \frac{1}{\xi} \nabla_y^s \underline{u} \left(\underline{x}, \underline{y} \right). \tag{26}$$

Similar developments as for the thermal problem can be performed as well, leading to the following results. $\underline{u}_0 = \underline{u}_M(\underline{x})$ is the macroscopic displacement, and $\varepsilon_M(\underline{x}) = \nabla_x^s \underline{u}_M$ is the macroscopic strain.
The microscopic problem can be defined as

$$\nabla_y \cdot \left(\mathbf{C} \nabla_y^s \underline{u}_1 \right) = -\nabla_y \cdot (\mathbf{C}\varepsilon_M) + \nabla_y \cdot (\mathbf{C}\alpha\theta_M \delta) \quad \text{in } \Omega_y, \tag{27}$$

which is parametrised by ε_M and θ_M, whose unknown $\underline{u}_1(\underline{x}, \underline{y})$ is y-periodic.
The macroscopic problem is

$$\begin{aligned} \nabla_x \cdot \sigma_M = 0 \quad &\text{in } \Omega, \\ \sigma_M = \langle \mathbf{C} \rangle_y \varepsilon_M + \left\langle \mathbf{C} \nabla_y^s \underline{u}_1 \right\rangle_y - \langle \mathbf{C}\alpha\delta \rangle_y \theta_M \quad &\text{in } \Omega, \\ \sigma_M \cdot \underline{n} = \underline{F}_d \quad &\text{on } \partial\Omega_{m2}, \\ \underline{u}_M = \underline{U}_d \quad &\text{on } \partial\Omega_{m1}. \end{aligned} \tag{28}$$

where σ_M is the macroscopic stress field.

As previously, the macro and micro problems are coupled. Finally, the total displacement field is approximated with the macroscopic part plus the first order micro-correction as $\underline{u}(\underline{x}, \underline{y}) = \underline{u}_M(\underline{x}) + \xi \underline{u}_1(\underline{x}, \underline{y})$, and the total strains and stresses are $\varepsilon(\underline{x}, \underline{y}) = \varepsilon_M(\underline{x}) + \nabla_y^s \underline{u}_1(\underline{x}, \underline{y})$ and $\sigma(\underline{x}, \underline{y}) = \mathbf{C}\left(\varepsilon - \alpha\theta_M \delta\right)$.

It is interesting to note that the mechanical problem is influenced only by the macroscopic temperature field and not by the higher order terms. The θ_1 term will appear in the mechanical problem only for higher order expansion mechanical terms, but not in this first-order correction.

4 Solution methodology

For the subsequent elucidations the spatial discretisation of both the macroscopic structure and microscopic unit-cell are performed using classical finite element method. Some of the parameters and operators used in the development are listed in table 1.

Table 1: Classical 3D FE parameters and operators

Parameter/ operator	Description
n_{nm}	Total number of nodes of the micro structure
n_{gm}	Total number of Gauss points of the micro structure
n_{nM}	Total number of nodes of the macro structure
n_{gM}	Total number of Gauss points of the macro structure
$[\mathrm{B}_z]$	$3n_{\mathrm{gm}} \times n_{\mathrm{nm}}$ matrix of shape function derivatives for the micro thermal problem
$[\mathrm{B}_q]$	$3n_{\mathrm{gm}} \times n_{\mathrm{nm}}$ matrix containing the integral of $[\mathrm{B}_z]$
$[k]$	$3n_{\mathrm{gm}} \times 3n_{\mathrm{gm}}$ diagonal matrix storing the micro thermal conductivity values at Gauss points
$[\mathrm{H}]$	$n_{\mathrm{nm}} \times n_{\mathrm{nm}}$ conductivity matrix of the micro thermal problem
$[\mathrm{C}]$	$n_{\mathrm{nm}} \times n_{\mathrm{nm}}$ capacity matrix of the micro thermal problem
$[\mathrm{B}_\varepsilon]$	$6n_{\mathrm{gm}} \times 3n_{\mathrm{nm}}$ matrix of shape function derivatives for the micro mechanical problem
$[\mathrm{B}_\sigma]$	$6n_{\mathrm{gm}} \times 3n_{\mathrm{nm}}$ matrix containing the integral of $[\mathrm{B}_\varepsilon]$
$[\mathbf{C}]$	$6n_{\mathrm{gm}} \times 6n_{\mathrm{gm}}$ block-diagonal matrix storing the micro elasticity tensor at Gauss points
$[\mathrm{K}]$	$3n_{\mathrm{nm}} \times 3n_{\mathrm{nm}}$ stiffness matrix of the micro mechanical problem

4.1 Thermal problem

A given unit cell can be considered for the following. Since the thermal micro problem (19) is linear, the solution is proportional to any given macroscopic gradient temperature vector $\underline{z}_M$. Therefore, there exists a linear operator $\mathcal{L}_{\mathrm{t}}$, called localisation operator, such that $\nabla_y \theta_1(\underline{y}) = -\mathcal{L}_{\mathrm{t}}(\underline{y})\underline{z}_M$. The heat flux (20) is now $\underline{q} = -k\left(\mathrm{I_d} - \mathcal{L}_{\mathrm{t}}\right)\underline{z}_M$ and its macroscopic part (24), $\underline{q}_M = -k_M \underline{z}_M$, where

$$k_M = \left\langle k\left(\mathrm{I_d} - \mathcal{L}_{\mathrm{t}}\right)\right\rangle_y \tag{29}$$

is the macroscopic homogenised conductivity tensor. This operator can be computed once for all during an offline phase for a given unit cell.

Once discretised with finite elements, the micro thermal problem reads

$$[\mathrm{H}]\{\theta_1\} = -\left[\mathrm{B}_q\right]^T [k]\,[B]\{z_M\} \quad \text{and} \quad \{z_1\} = [\mathrm{B}_z]\{\theta_1\}, \tag{30}$$

where additional y-periodicity has to be prescribed, as described in appendix A. $\{\theta_1\}$ is the $n_{\mathrm{nm}} \times 1$ column vector of nodal temperature unknowns, $\{z_1\}$ is the column vector storing the components of the temperature gradients at each Gauss point, whose size is $3n_{\mathrm{gm}} \times 1$. Finally, $\{z_M\}$ is a 3×1 column vector storing a single macro gradient, and $[B]$ is a boolean $3n_{\mathrm{gm}} \times 3$ mapping matrix, so that $[B]\{z_M\}$ is a full gradient column vector, uniform on every Gauss point. As $\left[\mathrm{B}_q\right]^T$ is the dual of $[\mathrm{B}_z]$, and indeed the conductivity matrix is $[\mathrm{H}] = \left[\mathrm{B}_q\right]^T [k]\,[\mathrm{B}_z]$, the dual of $[B]$ is denoted with $[D]^T$, which performs the integral over the micro-structure domain (see below).

To obtain numerically the discretised localisation operator $[\mathcal{L}_{\mathrm{t}}]$, whose size is $3n_{\mathrm{gm}} \times 3$, we load the unit cell with unitary uniform macro gradients. In 3D, this leads to 3 right hand sides, collected into the columns of the identity 3×3 matrix $[\mathrm{I_d}]$. 3 resolutions of the micro problem therefore leads to 3 temperature fields, whose gradients are the columns of the discretised localisation operator, so that

$$[\mathcal{L}_{\mathrm{t}}] = [\mathrm{B}_z]\left[\mathrm{H}\right]^{-1}\left[\mathrm{B}_q\right]^T [k]\,[B][\mathrm{I_d}], \tag{31}$$

(and one can discard the identity matrix in this expression). Finally, the macro homogenised conductivity tensor is

$$k_M = \frac{1}{V_y}[D]^T [k]\left([B] - [\mathcal{L}_{\mathrm{t}}]\right) \tag{32}$$

The macroscopic homogenised capacity is easily obtained by averaging

$$c_M = \langle \rho c \rangle_y \tag{33}$$

The core of the cost therefore resides in the 3 FE resolutions of a steady-state thermal problem on a unit cell.

The macroscopic thermal problem is a classical thermal transient problem using the previously computed macroscopic homogenised capacity c_M and conductivity k_M, of the form

$$[\mathrm{H}_M]\{\theta_M\} + [\mathrm{C}_M]\left\{\dot{\theta}_M\right\} = \{d\}, \tag{34}$$

where the right hand side $\{d\}$ contains the natural boundary conditions. $[\mathrm{H}_M]$ is the conductivity matrix built using the homogenised effective conductivity tensor k_M, and $[\mathrm{C}_M]$ is the capacity matrix obtained using the

homogenised heat capacity c_M. If the temporal integration scheme is the classical backward Euler method, then for a particular time step t_s, the problem to solve is

$$\left([\mathrm{H}_M] + \frac{1}{\Delta t} [\mathrm{C}_M] \right) \{\theta_M\}^s = \frac{1}{\Delta t} [\mathrm{C}_M] \{\theta_M\}^{s-1} + \{d\}^s , \tag{35}$$

where Δt is the time step.

4.2 Mechanical problem

The same uni cell is considered for the following development. Since the micro mechanical problem (27) is linear, the solution is a linear combination to any given macroscopic strain tensor ε_M and any given macroscopic temperature θ_M. Therefore, there exists two linear operators $\mathcal{L}_\mathrm{m}$ and $\mathcal{L}_\mathrm{mt}$, also called localisation operators, such that $\nabla_y^s \underline{u}_1(\underline{y}) = -\mathcal{L}_\mathrm{m}(\underline{y})\varepsilon_M + \mathcal{L}_\mathrm{mt}(\underline{y})\theta_M$. The total stress field is $\sigma = \mathbf{C}\,(\mathrm{I_d} - \mathcal{L}_\mathrm{m})\,\varepsilon_M - \mathbf{C}\,(\alpha\delta - \mathcal{L}_\mathrm{mt})\,\theta_M$ and its macroscopic part is $\sigma_M = \mathbf{C}_M\varepsilon_M - \mathbf{S}_M\theta_M$, where

$$\mathbf{C}_M = \langle \mathbf{C}\,(\mathrm{I_d} - \mathcal{L}_\mathrm{m}) \rangle_y \tag{36}$$

is the macroscopic homogenised elasticity tensor, and

$$\mathbf{S}_M = \langle \mathbf{C}\,(\alpha\delta - \mathcal{L}_\mathrm{mt}) \rangle_y \tag{37}$$

is a macroscopic homogenised effective coupling tensor. Note that a macroscopic homogenised expansion tensor can be defined as $\mathbf{A}_M = \mathbf{C}_M^{-1}\mathbf{S}_M$. These operators can be computed once for all during an offline phase for a given unit cell.

Once discretised with finite elements, the micro mechanical problem reads

$$[\mathrm{K}]\,\{u_1\} = -\,[\mathrm{B}_\sigma]^T\,[\mathbf{C}]\,[B_m]\{\varepsilon_M\} + [\mathrm{B}_\sigma]^T\,[\mathbf{C}]\,[B_m]\{\varepsilon_M^\mathrm{th}\} \quad \text{and} \quad \{\varepsilon_1\} = [\mathrm{B}_\varepsilon]\,\{u_1\}, \tag{38}$$

where additional y-periodicity has to be prescribed, as described in appendix A. $\{u_1\}$ is the $3n_\mathrm{nm} \times 1$ column vector of nodal displacement unknowns, $\{\varepsilon_1\}$ is the column vector storing the components of the strain tensors at each Gauss point, whose size is $6n_\mathrm{gm} \times 1$. The pre-strain is $\{\varepsilon_M^\mathrm{th}\} = \{\mathbf{A}_M\}\theta_M$. Finally, $\{\varepsilon_M\}$ is a 6×1 column vector storing the components of a single macro strain, and $[B_m]$ is a boolean $6n_\mathrm{gm} \times 6$ mapping matrix, so that $[B_m]\{\varepsilon_M\}$ is a full strain field column vector, uniform on every Gauss point. As $[\mathrm{B}_\sigma]^T$ is the dual of $[\mathrm{B}_\varepsilon]$, and the stiffness matrix $[\mathrm{K}] = [\mathrm{B}_\sigma]^T\,[\mathbf{C}]\,[\mathrm{B}_\varepsilon]$, the dual of $[B_m]$ is denoted with $[D_m]^T$, which performs the integral over the micro-structure domain (see below).

To obtain numerically the discretised localisation operators $[\mathcal{L}_\mathrm{m}]$ and $[\mathcal{L}_\mathrm{mt}]$, whose sizes are $6n_\mathrm{gm} \times 6$ and $6n_\mathrm{gm} \times 1$, we first load the unit cell with unitary uniform macro gradients. In 3D, this leads to 6 right-hand-sides, collected into the columns of the identity 6×6 matrix $[\mathrm{I_d}]$. 6 resolutions of the micro problem therefore leads to 6 displacement fields, whose strains are the columns of the first discretised localisation operator. Second, we load the unit cell with a uniform macro temperature field to get the second localisation operator. This reads

$$[\mathcal{L}_\mathrm{m}] = [\mathrm{B}_\varepsilon]\,[\mathrm{K}]^{-1}\,[\mathrm{B}_\sigma]^T\,[\mathbf{C}]\,[B_m]\,[\mathrm{I_d}] \quad \text{and} \quad [\mathcal{L}_\mathrm{mt}] = [\mathcal{L}_\mathrm{m}]\,\{\mathbf{A}_M\}, \tag{39}$$

(and one can discard the identity matrix in the first expression). Finally, the macro homogenised tensors are

$$\mathbf{C}_M = \frac{1}{V_y}[D_m]^T\,[\mathbf{C}]\,([B_m] - [\mathcal{L}_\mathrm{m}]) \quad \text{and} \quad \mathbf{S}_M = \mathbf{C}_M\{\mathbf{A}_M\}. \tag{40}$$

The core of the cost therefore resides in the 6 FE resolutions of an elastic problem on a unit cell. The macroscopic mechanical problem is a classical elastic problem subjected to a thermal pre-strain using the previously computed macroscopic homogenised elasticity tensor and expansion tensor.

The macroscopic mechanical problem is a classical elastic problem using the previously computed macroscopic homogenised elastic tensor $\mathbf{C}_M$ and coupling tensor $\mathbf{S}_M$, of the form

$$[\mathrm{K}_M]\,\{u_M\}^s = \{f\}^s + [\mathrm{B}_{\sigma M}]^T\,[\mathbf{S}_M]\,[\mathrm{B}_{\theta M}]\,\{\theta_M\}^s , \tag{41}$$

where the right hand side $\{f\}$ contains the natural boundary conditions. $[\mathrm{K}_M]$ is the stiffness matrix build using the homogenised effective elasticity tensor $\mathbf{C}_M$, and $[\mathrm{B}_{\theta M}]$ interpolates the nodal temperature values to the Gauss points.

When considering variable micro-structures, the macroscopic problem can be considered to be of macroscopic material with gradient of properties. To satisfy the quasi-periodic assumption of the underlying micro-structures, this gradient should nevertheless exhibit length scales related to the macroscopic one. The material parameters, including the micro-structural ones, are therefore defined as fields at macro scale only. The direct application of the previous methodology would lead to compute the micro-problems for each different unit cell, so potentially for each macroscopic Gauss points, which is very expensive. The idea to be more frugal is elucidated subsequently.

4.3 Variation in material properties

A very particular case where the material properties of the unit cells are assumed to vary proportionally between macroscopic Gauss points is considered herein. This case is considered as a test case for the multi-scale POD strategy, and can be of interest in material optimisation design (e.g. a 3D printing material manufacturing, embedding a mixture of constituents for each phase – multi-material multi-nozzle 3D printing; the optimisation process will be performed with this constituent ratio as a single design variable).

Though the macroscopic material characteristics are variable from one macroscopic Gauss point to another, only one representative resolution of the microscopic problem is enough and only thing needed is the gradient of variation. Indeed, the proportionality assumption is first traduced as the presence of only one independent micro-structural parameter, say $\varsigma(\underline{x})$. Second, is the unit cell with parameter value ς_0 is considered to be a representative problem, with the corresponding values of micro material characteristics $(\rho c)_0$, k_0 for the thermal problem and Young modulus E_0 and thermal expansion α_0 for the mechanical problem, then all the previous FE matrices for the left-hand sides, and behaviours are varying proportionally with ς/ς_0 ratio, so does all the relocalisation parameters and macroscopic computed homogenised parameters; for instance, one gets $\mathbf{C}_M(\varsigma) = \frac{\varsigma}{\varsigma_0}\mathbf{C}_M(\varsigma_0)$.

This particular case effectively reduces the unit cell problems into computation of only one representative unit cell. Now if additionally, the geometric properties are considered to be variable, a different strategy must be employed.

4.4 Variation in geometric properties

Only the fibre radius $\vartheta(\underline{x})$ is considered here as a variable parameter. This case is also considered as a simplification. Note however that if the fibre orientation is also involved, it is only a parameter field at macro-scale: the cell behaviour can be performed in the known eigenframe, aligned with the local fibre orientation, thanks to the quasi-periodic assumption.

Now the full order solution, as mentioned before, requires the resolution of the microscopic problem (as well as generation of mesh) n_{gM} times (n_{gM} being the total number of macroscopic Gauss points).

A suited strategy is to use a classical sampling method to build a reduced order model as a surrogate model. A few micro-structural meshes corresponding to certain values of the parameter ϑ_i, $i = 1 \dots p$, are generated, for $p \ll n_{\mathrm{gM}}$. The microscopic problems now need to be solved p times to generate, in an offline phase, p values for the quantities of interest, here the macroscopic homogenised characteristics. The online phase, the resolutions of the macroscopic problems, will require the values of these quantities of interest at the n_{gM} macroscopic points. This is performed via costless n_{gM} interpolations between the samples/snapshots of the offline phase. For instance, at a macroscopic Gauss point located at coordinates $\underline{x}$, i.e. supporting the parameter value $\vartheta(\underline{x})$, the characteristic $\mathbf{C}_M(\vartheta)$ is obtained via a 1D interpolation of the reduced model for the dependence to the parameter of the heuristic pre-computed law $(\vartheta_i, \mathbf{C}_{M,i})_{i=1\dots p}$.

The rest of the procedure is the same as described before.

If both variations are involved (linear dependence for material parameters and non-linear dependence to geometric parameter), the two previous strategies can easily be combined together. Once cost has been reduced for the micro problems with these strategies, the computation bottleneck may also arise in the online solving phase for the macroscopic problems. The next step is therefore to further reduce this computational cost using a reduced order strategy in the online macroscopic stage.

4.5 Proper Orthogonal Decomposition

The basic use of Proper Orthogonal Decomposition (POD) is to compute certain full-order problems in order to extract relevant information which can then be used to calculate similar problems more efficiently. In a nutshell the idea herein is to solve the full order macroscopic problems (both thermal and mechanical) for initial few time steps and obtain the solution as snapshots. Thereafter these snapshots can be used to built a projection matrix that projects the solution in the POD subspace. This projection matrix can be used to solve the problems for the remaining time steps, but in a reduced space.

One way of building a projection matrix is to find the eigenvectors of the covariant matrix. Considering $[\upsilon]$ to store the solution fields in its columns, which is of size $d_{\mathrm{f}} \cdot n_{\mathrm{nM}} \times n_{\mathrm{t}}$ (n_{t} being the number of the selected initial time steps and d_{f} the number of degrees of freedom per node), the covariant matrix [M] can be obtained by

$$[\mathrm{M}] = [\upsilon]\,[\upsilon]^T\,. \tag{42}$$

After that an eigenvalue analysis gives the eigenvectors, from which only a few major eigenvectors are selected (depending on the major eigenvalues) to obtain the projection matrix [P] which of size $d_{\mathrm{f}} \cdot n_{\mathrm{nM}} \times q$, where $q \ll d_{\mathrm{f}} \cdot n_{\mathrm{nM}}$ (in practice, the same result can be obtained in a robust way using a SVD on $[\upsilon]$ directly).

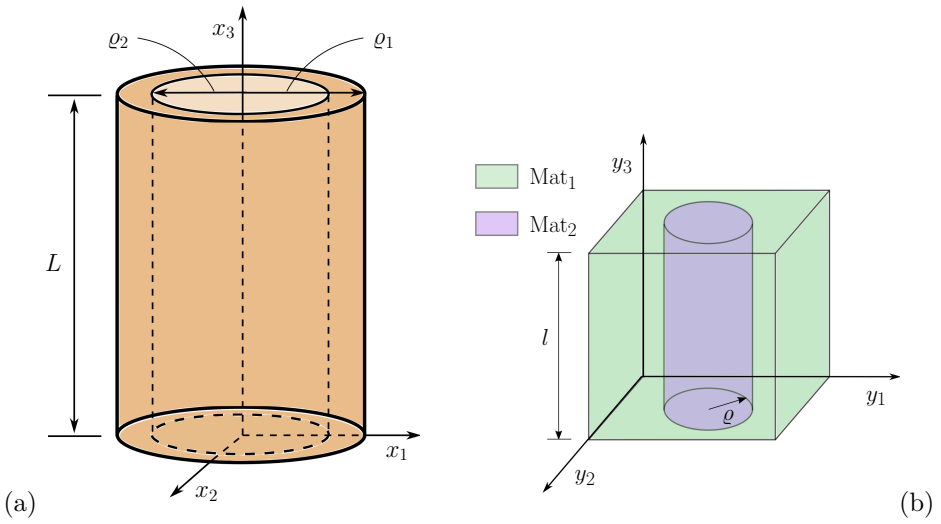

Figure 2: (a) Macroscopic structure, and (b) microscopic structure

Once the projection matrix is built, the idea is to use it to solve the problem for all the remaining time steps in a reduced domain.

For a given time step t_s, the equation to solve is of the form

$$[\Lambda]\{\upsilon\}^s = \{W\}^s, \tag{43}$$

where the left hand side $[\Lambda]$ has for size $d_\mathrm{f}\cdot n_\mathrm{nM} \times d_\mathrm{f}\cdot n_\mathrm{nM}$, and the right hand side $\{W\}^s$ has for size $d_\mathrm{f}\cdot n_\mathrm{nM}\times 1$. $\{\upsilon\}^s$ is a generalised nodal unknown of size $d_\mathrm{f}\cdot n_\mathrm{nM}\times 1$.

The nodal unknowns can be searched in an approximate form using the reduced nodal unknown $\{\upsilon_\mathrm{red}\}^s$ with the smaller size $q\times 1$:

$$\{\upsilon\}^s = [\mathrm{P}]\{\upsilon_\mathrm{red}\}^s, \tag{44}$$

The corresponding variational form of (43) leads to the reduced-size problem

$$[\Lambda_\mathrm{red}]\{\upsilon_\mathrm{red}\}^s = \{W_\mathrm{red}\}^s, \tag{45}$$

where $[\Lambda_\mathrm{red}] = [\mathrm{P}]^T[\Lambda][\mathrm{P}]$ is of size $q\times q$ and $\{W_\mathrm{red}\}^s = [\mathrm{P}]^T\{W\}^s$ is of size $q\times 1$. Eq. (45) basically means that at each time step instead of solving $d_\mathrm{f}\cdot n_\mathrm{nM}$ linear equations, only q equations are solved.

The proposed strategy takes advantage of the initial time step full order solutions, that are expected to contain a strong transient part of the evolution, therefore containing a rich information. It could nevertheless happen that this information is not sufficient for accurate solutions of further time steps. To check this, an adaptive strategy can be designed: an incremental error estimator can be built from time to time by computing the residual of the full order problem (43) on a solution (44) of the reduced order problem (45), in order to decide if a new full order solution is required, that can contribute to enrich the reduced space, in an adaptive manner. This variant has not been needed on the following examples, and is a direct perspective to this approach. In the current study, this therefore boils down to a classical *a posteriori* reduced-basis approach [31, 23].

5 Numerical example

A cylindrical pipe as shown in fig. 2(a) is considered for a demonstrative example. The geometry of the structure is given with the length of the pipe $L = 0.5\,\mathrm{m}$, the outer radius $\varrho_1 = 0.1\,\mathrm{m}$ and the inner radius $\varrho_2 = 0.05\,\mathrm{m}$. The outer surface of the pipe is subjected to a fixed temperature $\theta_f = 0\,^\circ\mathrm{C}$. A temperature $\theta_d = 200\sin(2\pi t/\mathcal{T})\,^\circ\mathrm{C}$ of time period $\mathcal{T} = 10^4\,\mathrm{s}$ is prescribed on the inner surface of the pipe for 1 cycle. Here the loading is only of thermal nature, and we study the thermo-mechanical response that arises from it.

The underlying micro-structure shown in fig. 2(b) consists of a cube of length $l = 1\times 10^{-5}\,\mathrm{m}$ (so the scale ratio is $\xi = l/L = 2\times 10^{-5}$). The majority of the cube is made of material Mat$_1$, while a cylindrical portion of radius ϑ is composed of material Mat$_2$, see fig. 2(b). Now the variation of material properties is ruled by the parameter $\varsigma(\underline{x}) = \varsigma_0\left(1+\frac{0.25}{L}(x_1+x_2+x_3)\right)$, where $\varsigma = \{E, \rho c, k, \alpha\}$ and ς_0 represents the base values of the material properties. The Poisson's ratio ν however is considered to be a constant at 0.3.

The macroscopic structure is discretised using 360 linear 8 noded isoparametric hexahedral elements with 8 Gauss points per element. This constitutes of a total of 560 nodes and 2880 Gauss points.

Two test cases are presented subsequently.

Table 2: Base values of material properties

Parameters	Mat_1	Mat_2
E_0 / Pa	210×10^9	190×10^9
$\rho c_{t\,0}$ / $(\text{Jm}^{-3}\text{K}^{-1})$	3978×10^3	3588×10^3
$k_{t\,0}$ / $(\text{Wm}^{-1}\text{K}^{-1})$	45	12
α_0 / (K^{-1})	1×10^{-5}	1.6×10^{-5}

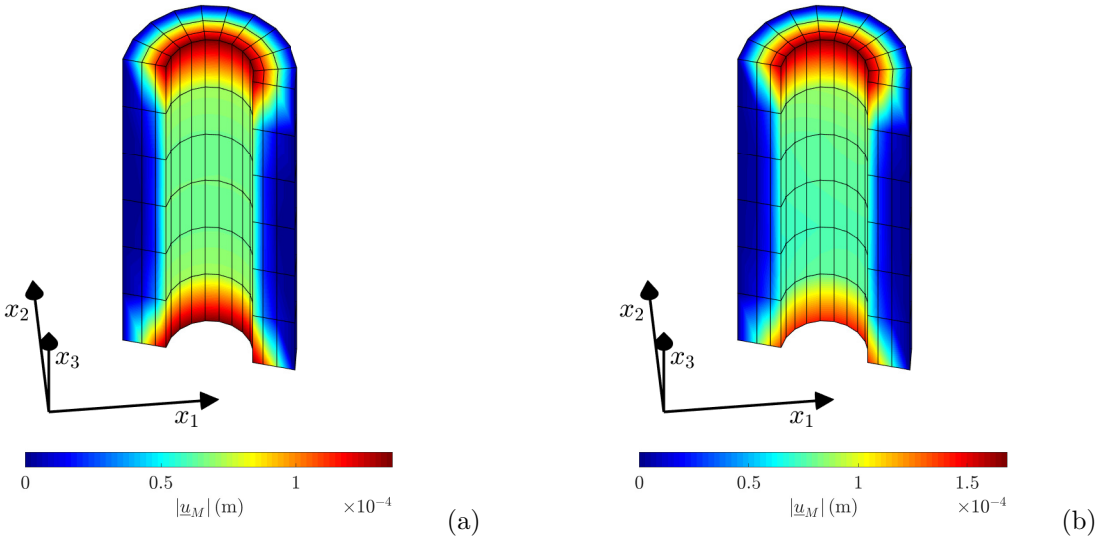

Figure 3: Magnitude of macroscopic displacement. (a) Using identical unit cells. (b) Using variable unit cells.

5.1 Material variation test

For the first study we consider variation only of material properties, and the fibre radius is fixed at $\vartheta = 0.3 \times 10^{-5}\,\text{m}$. For a single micro-structure, 1700 elements are used, that result in a total of 2262 nodes and 13600 Gauss points.

For the micro-problem, if the multipliers described in Section 4.3 are used, the total simulation time for the unit cell problems is 0.04% of the time needed if all the 2880 unit cells are solved individually. In addition to the frugality of the micro-problems, the macro-problems are solved using POD providing further time savings. The temporal path of the problem is discretised using 100 time steps. The training stage was calculated for initial first 10 time steps and, as the problem is linear, the projection matrix obtained from the snapshots is enough to calculate the remaining time steps in a reduced space. Only five POD modes (i.e. $q = 5$) are enough for both the thermal and the mechanical problems. For a particular time step the simulation cost of the mechanical problem using the reduced order method is 2.5% of the simulation time of the full order problem.

For comparison purposes, a separate simulation is performed for identical unit cells using the base values of the material properties. The following figures show the maps of certain quantities of interest at a time point where θ_d is maximum. For the macroscopic quantities, half of the pipe is shown to visualise the inner field. Fig. 3 shows the magnitude macroscopic displacements. It is clear that variable unit cells produces a higher displacement magnitude, and the top and bottom region is asymmetric. Fig. 4 shows the macroscopic von Mises stress. Similar to Fig. 3, the quantity of interest is asymmetric with respect to x_3 axis along with higher stresses for the variable unit cell case. The Gauss points for the two cases where the stress is maximum are different, the underlying micro-structures are shown in Fig. 5. Fig. 6 shows the magnitude of the macroscopic heat flux density. Similar to stress, the quantity of interest is asymmetric with respect to x_3 axis along with higher values for the variable unit cell case. The Gauss points for the two cases where the quantity is maximum are different, the underlying micro-structures are shown in Fig. 7.

For an assessment of the accuracy of the POD at macro scale, a full order solution (without POD) is also computed for variable unit cells and the relative errors obtained are $er_\theta = 8.8 \times 10^{-8}$ and $er_\sigma = 9.2 \times 10^{-8}$, where the relative errors are defined as

$$er_\sigma = \frac{\|\sigma_M^{\text{fo}} - \sigma_M^{\text{ro}}\|}{\|\sigma_M^{\text{fo}}\|}, \quad er_\theta = \frac{\|\theta_M^{\text{fo}} - \theta_M^{\text{ro}}\|}{\|\theta_M^{\text{fo}}\|}, \tag{46}$$

with superscripts 'ro' and 'fo' representing the reduced order and full order solutions. It is clear through the values of the relative errors that the reduced bases obtained through the training stage are enough to solve the total problem in a reduced space with high accuracy.

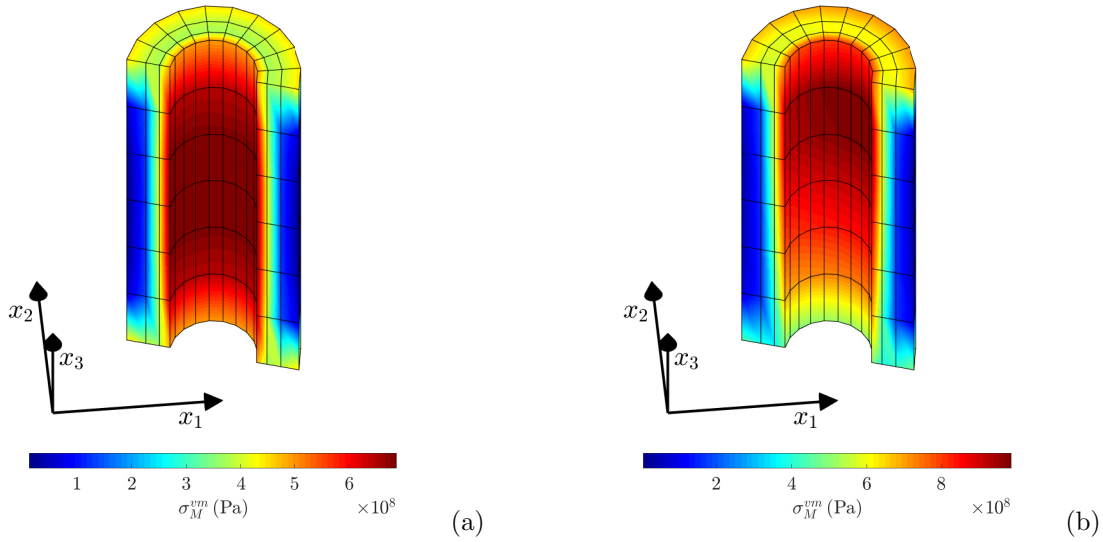

Figure 4: Macroscopic von Mises stress. (a) Using identical unit cells. (b) Using variable unit cells.

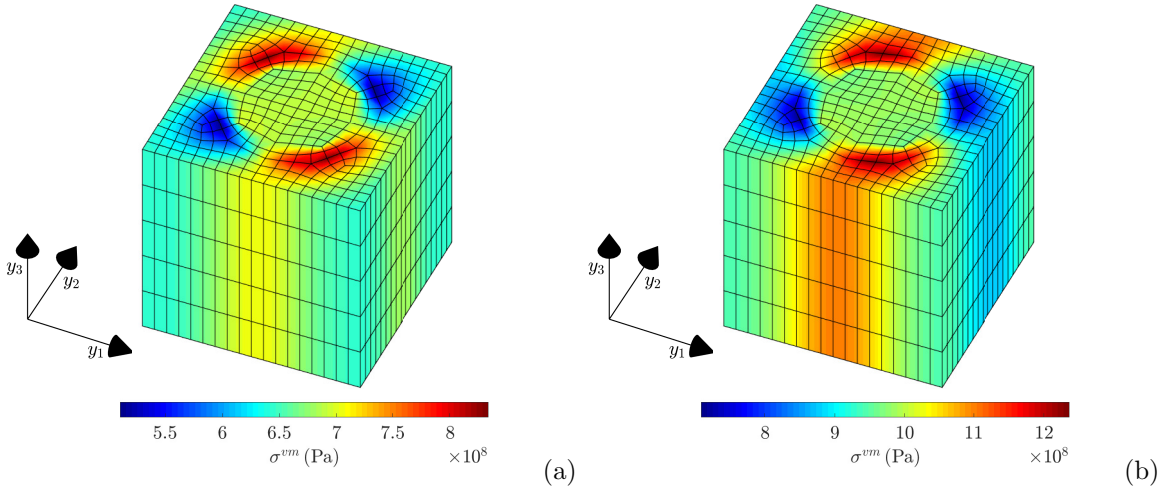

Figure 5: Microscopic von Mises stress. (a) Using identical unit cells. (b) Using variable unit cells.

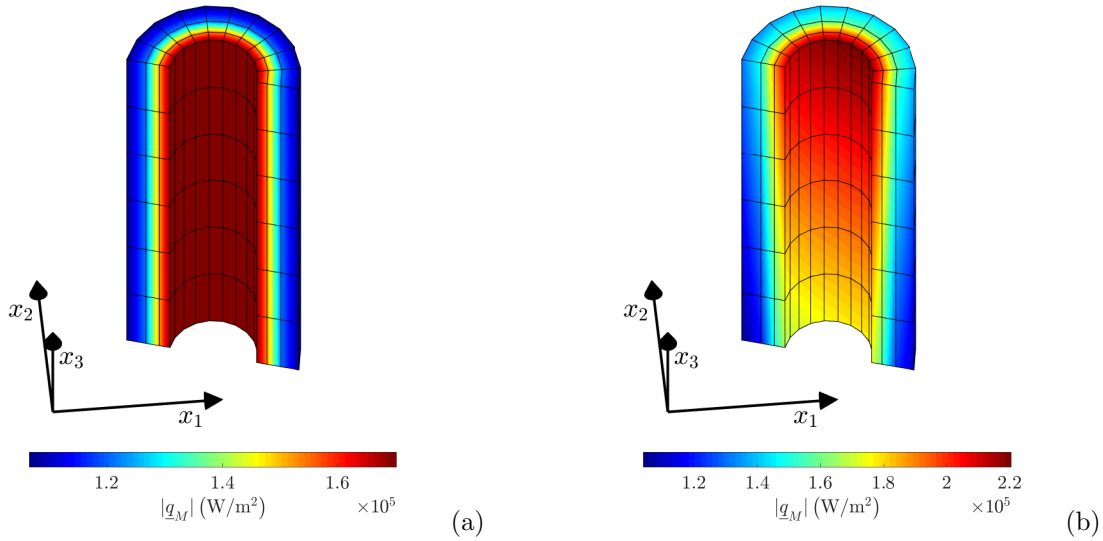

Figure 6: Magnitude of macroscopic heat flux density. (a) Using identical unit cells. (b) Using variable unit cells.

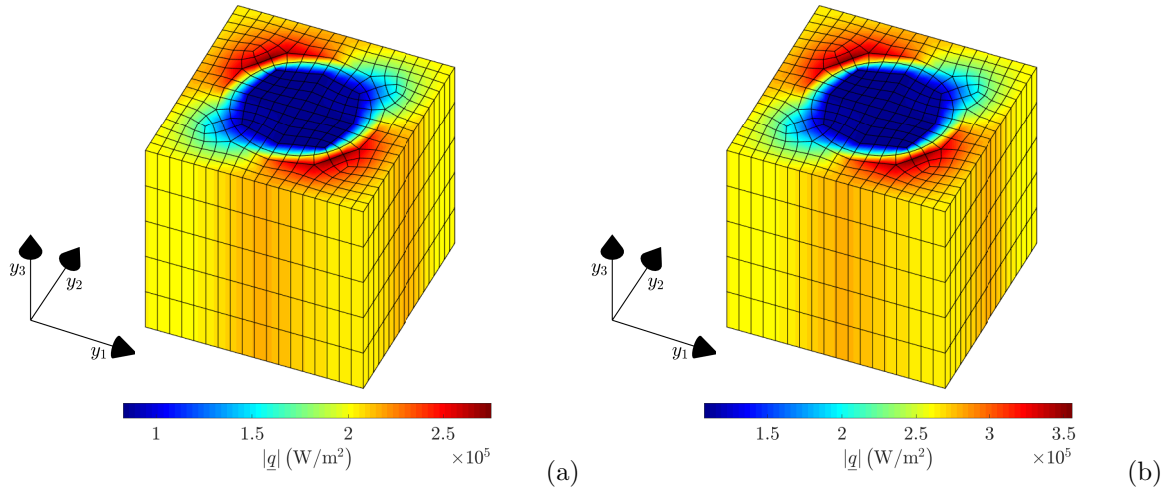

Figure 7: Magnitude of microscopic heat flux density. (a) Using identical unit cells. (b) Using variable unit cells.

5.2 All variations test

For the second study, we consider variations of material as well as geometric properties. The fibre diameter is now considered to vary between 0.2×10^{-5} m and 0.4×10^{-5} m. Consider the sampling method as mentioned in Section 4.4, the fibre diameters of the micro-structures and their locations at specific macro GPs are given in table 3 (the overall spatial distribution is given in Fig. 8).

Table 3: Specific radii and corresponding macro GPs

fibre radius	macro GP number	macro GP location
0.20×10^{-5} m	1	$(-0.0549, 0.0346, 0.4824)$ m
0.22×10^{-5} m	100	$(-0.0346, 0.0548, 0.4824)$ m
0.24×10^{-5} m	300	$(0.0415, 0.0499, 0.3991)$ m
0.26×10^{-5} m	500	$(0.0602, -0.0241, 0.3157)$ m
0.28×10^{-5} m	800	$(-0.0415, -0.0498, 0.1843)$ m
0.30×10^{-5} m	1200	$(-0.0054, 0.0816, 0.0176)$ m
0.32×10^{-5} m	1800	$(-0.0630, -0.0524, 0.2676)$ m
0.34×10^{-5} m	2000	$(-0.0377, -0.0453, 0.1843)$ m
0.36×10^{-5} m	2300	$(0.0548, -0.0219, 0.0657)$ m
0.38×10^{-5} m	2500	$(0.0219, 0.0548, 0.4824)$ m
0.40×10^{-5} m	2880	$(-0.0572, -0.0145, 0.0176)$ m

So there are 11 micro-structural samples. Concerning their FE discretisations, 1000 to 1820 elements are used, that results in a total of 1374 to 2406 nodes and 8000 to 14560 Gauss points. Basically instead of 2880 micro structural calculations only 11 are used, which estimates about 99.6% of cost saving. For testing purpose, the fibre diameter is considered to be varying according to the ordinal number of the macro GPs.

Fig. 9, Fig. 10 and Fig. 12 show the macroscopic von Mises stress, heat flux density and the displacement, respectively. Relocalisation is however tricky as all the micro-structural meshes are not available so relocalisation is possible only at the sampling points. In this case the micro-structure corresponding to macro GP number 1200 is chosen (see Fig. 12 and Fig. 13).

6 Conclusion

This article introduces a multi-scale method based on asymptotic theory to compute thermo-elasticity for heterogeneous structures containing quasi-periodic micro-structures. To avoid simulation of all the micro-structural unit cells, linear operators were defined that relates the microscopic quantities with their macroscopic counterparts. This particular procedure was extended for variable unit cells using scalar multiples and interpolations. This reduces the simulation cost drastically as only one single representative unit cell had to be computed for material variations and few sample micro-structures for geometric variations. Finally a POD-based reduced

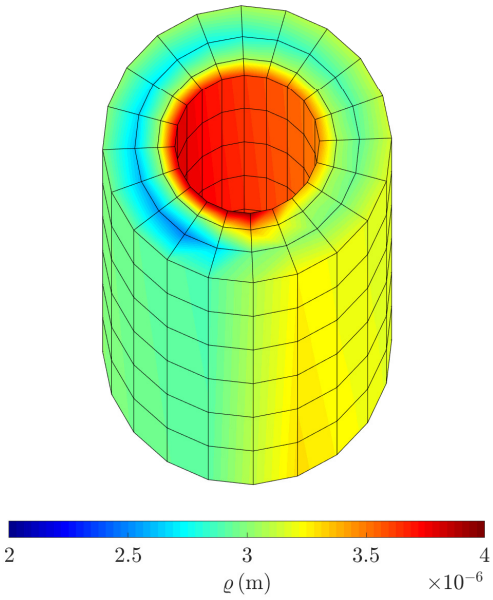

Figure 8: Variation of fibre diameter with respect to the macro-structure.

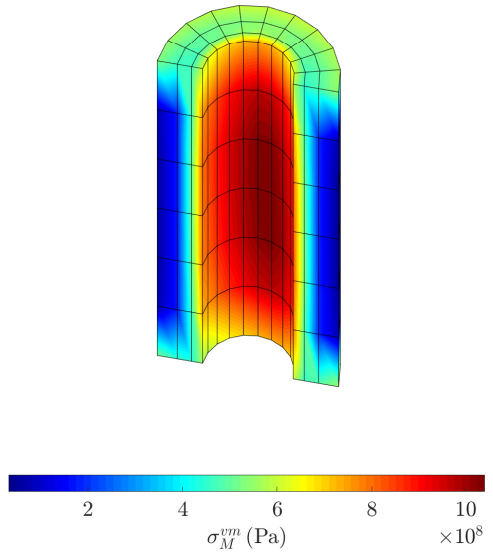

Figure 9: Macroscopic von Mises stress using micro-structures of different radii and material properties.

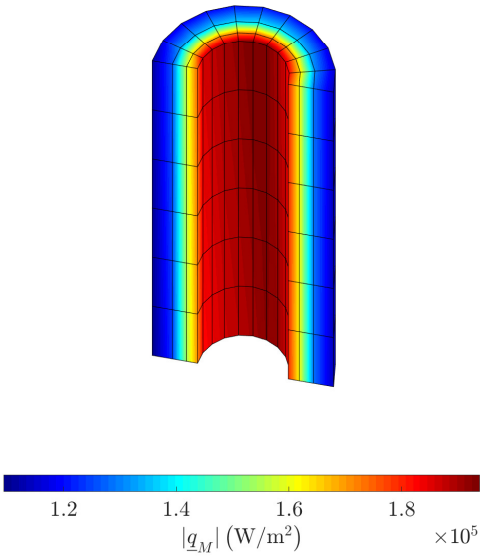

Figure 10: Magnitude of macroscopic heat flux density using micro-structures of different radii and material properties.

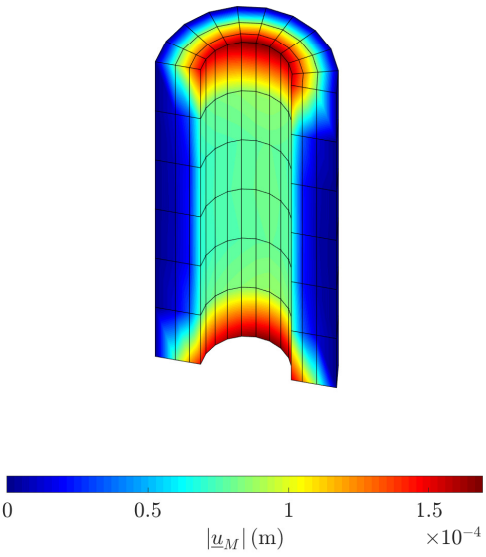

Figure 11: Magnitude of macroscopic displacement using micro-structures of different radii and material properties.

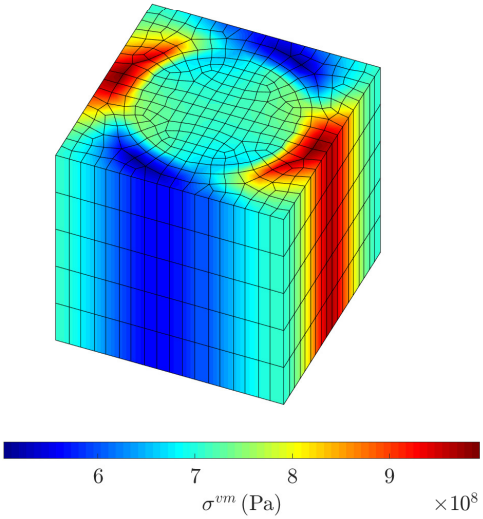

Figure 12: Microscopic von Mises stress at a unit cell underlying macro GP number 1200 using micro-structures of different radii and material properties.

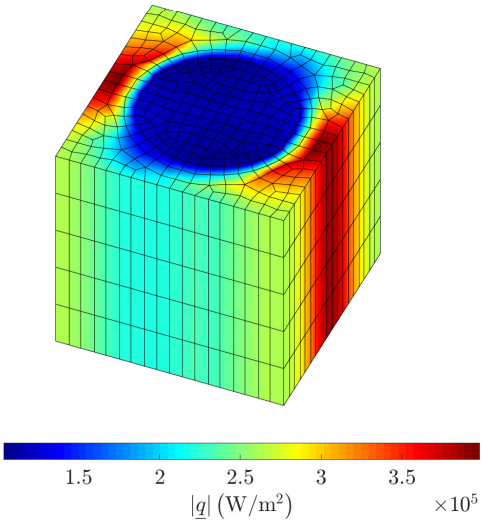

Figure 13: Magnitude of microscopic heat flux density at a unit cell underlying macro GP number 1200 using micro-structures of different radii and material properties.

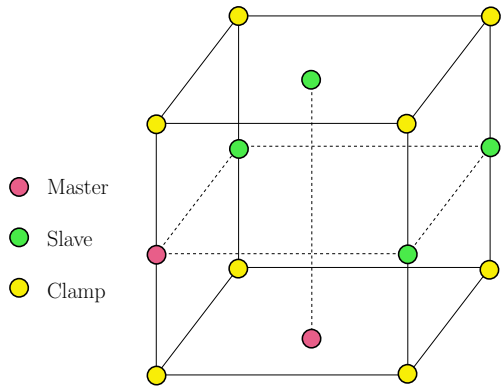

Figure 14: Unit cell indicating master-slave nodes

order strategy is used to reduce the cost of the macroscopic problem. This particular version of POD as well as the usage of linear operators are conducive as this particular problem is linear. In case of non-linear problems, even if the global solution is computed in a reduced space, the computational effort to solve the non-linear constitutive relation at every local integration point remains high. To put that in perspective, the local computations are independent of the reduced model and the reduced approximation has no influence on the numerical expense with regard to the estimation of the internal variables that influence the tangent stiffness matrix. For such cases classical POD will not provide reasonable cost reduction, and methods like hyper-reduction [37] or empirical interpolation method [36] are more suited.

Using this type of unified approach is also suitable for cases where stochastic samplings are needed, where the deterministic problem is used as black box with the solution being calculated in a reduced space (extremely cheap). Inverse problems like optimisation are also under concern.

However care should be taken that material/geometric parameters, boundary conditions do not alter too much for the samples so that new training stages are not required, unless adaptivity control is embedded.

Other perspectives concern the case where more parameters are involved. Some solution strategies consist in switching from SVD to Higher Order SVG (HO-SVD) [6], Higher Order Proper Generalized Decomposition (HO-PGD) [30, 24], Candecomp/Parafac (CP) [8], or their gappy versions [42, 43]. Other surrogate modellings can be considered, such as Kriging [39], or even Support Vector Regression (SVR) [5]. Other perspective is to tackle some different physical modeling, for instance cases where the micro-structure is so small, and loadings with high frequency, that may lead to dynamic mechanical effects, or even thermal waves, for which some homogenization techniques are also available [46].

A Construction of periodicity matrix

The resolution of the unit cell problems basically boils down to the resolution of a generalised form $[\mathrm{X}]\,\{\eta\} = \{r\}$, both for the thermal (30) and mechanical (38) micro problems.

To impose the periodicity condition, a substitution matrix [G] is constructed based on the master-slave node pairs, fig. 14. This matrix can be used to reduce the linear system to $[\mathrm{X}_{\mathrm{red}}]\,\{\eta_{\mathrm{red}}\} = \{r_{\mathrm{red}}\}$, where $[\mathrm{X}_{\mathrm{red}}] = [\mathrm{G}]^T\,[\mathrm{X}]\,[\mathrm{G}]$, $\{r_{\mathrm{red}}\} = [\mathrm{G}]^T\,\{r\}$ and $\{\eta\} = [\mathrm{G}]\,\{\eta_{\mathrm{red}}\}$.

The construction of the periodicity matrix [G] is based on the number of master-slave nodes that ensures periodicity. Consider a representative unit cell as shown fig. 14. The periodicity condition requires that nodal unknowns at each surface be identical to the nodal unknowns of its opposite surface. It is necessary to have the nodal distributions at a particular surface should be identical to its opposite surface. Consider a particular surface be a master surface and its opposite be its slave. Then each node of the master surface, will have its slave counterpart on the opposite surface. As far as the edges are concerned, it is necessary to have the nodal distribution of a particular edge be identical to all three of its parallel edges. In this case for a node of a master edge there will be three slave nodes on the other three parallel edges.

Finally, the eight corner nodes should have the same nodal value. But since the genuine system to solve in undetermined ([X] has a non void kernel, whose right hand side is orthogonal) it is necessary and sufficient to clamp these corner nodes.

The matrix [G] represents these substitutions, duplicating values attached to master node to slave nodes. It therefore reduces the size of the system by substitution, getting rid of degrees of freedom related to slave and clamp nodes.

This nevertheless requires that the mesh is generated while ensuring the node-to-node correspondence on opposite faces.

References

[1] A. Bensoussan, J.-L. Lions, and G. Papanicolaou. *Asymptotic Analysis for Periodic Structures*. American Mathematical Society, Providence, R.I, 2011. doi:10.1090/chel/374.

[2] Mainak Bhattacharyya, David Dureisseix, and Beatrice Faverjon. Numerical homogenisation based on asymptotic theory and model reduction for coupled elastic-viscoplastic damage. *International Journal of Damage Mechanics*, 29(9):1416–1444, jun 2020. doi:10.1177/1056789520930785.

[3] Mainak Bhattacharyya, Amélie Fau, Rodrigue Desmorat, Shadi Alameddin, David Néron, Pierre Ladevèze, and Udo Nackenhorst. A kinetic two-scale damage model for high-cycle fatigue simulation using multi-temporal Latin framework. *European Journal of Mechanics - A/Solids*, 77:103808, sep 2019. doi:10.1016/j.euromechsol.2019.103808.

[4] Anindya Chatterjee. An introduction to the proper orthogonal decomposition. *Current Science*, 78:808–817, 2000.

[5] Stella M. Clarke, Jan H. Griebsch, and Timothy W. Simpson. Analysis of support vector regression for approximation of complex engineering analyses. volume Volume 2: 29th Design Automation Conference, Parts A and B of *International Design Engineering Technical Conferences and Computers and Information in Engineering Conference*, pages 535–543. ASME, 09 2003. doi:10.1115/detc2003/dac-48759.

[6] Lieven De Lathauwer, Bart De Moor, and Joos Vandewalle. A multilinear singular value decomposition. *SIAM Journal on Matrix Analysis and Applications*, 21(4):1253–1278, jan 2000. doi:10.1137/s0895479896305696.

[7] F. Devries, H. Dumontet, G. Duvaut, and F. Lene. Homogenization and damage for composite structures. *International Journal for Numerical Methods in Engineering*, 27(2):285–298, 1989. doi:10.1002/nme.1620270206.

[8] Nicolaas M. Faber, Rasmus Bro, and Philip K. Hopke. Recent developments in CANDECOMP/PARAFAC algorithms: a critical review. *Chemometrics and Intelligent Laboratory Systems*, 65(1):119–137, jan 2003. doi:10.1016/s0169-7439(02)00089-8.

[9] F. Feyel. Multiscale FE2 elastoviscoplastic analysis of composite structures. *Computational Materials Science*, 16(1):344–354, 1999. doi:10.1016/s0927-0256(99)00077-4.

[10] Frédéric Feyel and Jean-Louis Chaboche. FE2 multiscale approach for modelling the elastoviscoplastic behaviour of long fibre SiC/Ti composite materials. *Computer Methods in Applied Mechanics and Engineering*, 183(3):309–330, 2000. doi:10.1016/s0045-7825(99)00224-8.

[11] Jacob Fish, Kamlun Shek, Muralidharan Pandheeradi, and Mark S. Shephard. Computational plasticity for composite structures based on mathematical homogenization: Theory and practice. *Computer Methods in Applied Mechanics and Engineering*, 148(1-2):53–73, 1997. doi:10.1016/s0045-7825(97)00030-3.

[12] Jacob Fish and Amir Wagiman. Multiscale finite element method for a locally nonperiodic heterogeneous medium. *Computational Mechanics*, 12(3):164–180, May 1993. doi:10.1007/bf00371991.

[13] Jacob Fish, Qing Yu, and Kamlun Shek. Computational damage mechanics for composite materials based on mathematical homogenization. *International Journal for Numerical Methods in Engineering*, 45(11):1657–1679, 1999. doi:10.1002/(sici)1097-0207(19990820)45:11<1657::aid-nme648>3.0.co;2-h.

[14] Samuel Forest, Francis Pradel, and Karam Sab. Asymptotic analysis of heterogeneous Cosserat media. *International Journal of Solids and Structures*, 38(26-27):4585–4608, 2001. doi:10.1016/s0020-7683(00)00295-x.

[15] Felix Fritzen, Samuel Forest, Thomas Böhlke, Djimedo Kondo, and Toufik Kanit. Computational homogenization of elasto-plastic porous metals. *International Journal of Plasticity*, 29:102–119, 2012. doi:10.1016/j.ijplas.2011.08.005.

[16] Felix Fritzen and Max Hodapp. The finite element square reduced (FE2R) method with GPU acceleration: towards three-dimensional two-scale simulations. *International Journal for Numerical Methods in Engineering*, 107(10):853–881, 2016. doi:10.1002/nme.5188.

[17] Marc G. D. Geers, Varvara G. Kouznetsova, Karel Matous, and Julien Yvonnet. *Homogenization Methods and Multiscale Modeling: Nonlinear Problems*, pages 1–34. John Wiley and Sons Ltd., 2017. doi:10.1002/9781119176817.ecm2107.

[18] Ronen Haymes and Erez Gal. Iterative multiscale approach for heat conduction with radiation problem in porous materials. *Journal of Heat Transfer*, 140(8), apr 2018. doi:10.1115/1.4039420.

[19] Marcin Kaminski. Homogenization of transient heat transfer problems for some composite materials. *International Journal of Engineering Science*, 41(1):1–29, jan 2003. doi:10.1016/S0020-7225(02)00144-1.

[20] V. Kouznetsova, W. A. M. Brekelmans, and F. P. T. Baaijens. An approach to micro-macro modeling of heterogeneous materials. *Computational Mechanics*, 27(1):37–48, Jan 2001. doi:10.1007/s004660000212.

[21] V. Kouznetsova, M. G. D. Geers, and W. A. M. Brekelmans. Multi-scale constitutive modelling of heterogeneous materials with a gradient-enhanced computational homogenization scheme. *International Journal for Numerical Methods in Engineering*, 54(8):1235–1260, 2002. doi:10.1002/nme.541.

[22] Matthias Leuschner and Felix Fritzen. Reduced order homogenization for viscoplastic composite materials including dissipative imperfect interfaces. *Mechanics of Materials*, 104:121–138, 2017. doi:10.1016/j.mechmat.2016.10.008.

[23] Y. C. Liang, H. P. Lee, S. P. Lim, W. Z. Lin, K. H. Lee, and C. G. Wu. Proper orthogonal decomposition and its application - Part I: theory. *Journal of Sound and Vibration*, 252(3):527–544, may 2002. doi:10.1006/jsvi.2001.4041.

[24] Y. Lu, N. Blal, and A. Gravouil. Adaptive sparse grid based HOPGD: Toward a nonintrusive strategy for constructing space-time welding computational vademecum. *International Journal for Numerical Methods in Engineering*, 114(13):1438–1461, mar 2018. doi:10.1002/nme.5793.

[25] Xanthippi Markenscoff and Cristian Dascalu. Asymptotic homogenization analysis for damage amplification due to singular interaction of micro-cracks. *Journal of the Mechanics and Physics of Solids*, 60(8):1478–1485, 2012. doi:10.1016/j.jmps.2012.04.004.

[26] A. Matine, N. Boyard, P. Cartraud, G. Legrain, and Y. Jarny. Modeling of thermophysical properties in heterogeneous periodic media according to a multi-scale approach: Effective conductivity tensor and edge effects. *International Journal of Heat and Mass Transfer*, 62:586–603, jul 2013. doi:10.1016/j.ijheatmasstransfer.2013.03.036.

[27] A. Matine, N. Boyard, G. Legrain, Y. Jarny, and P. Cartraud. Transient heat conduction within periodic heterogeneous media: A space-time homogenization approach. *International Journal of Thermal Sciences*, 92:217–229, jun 2015. doi:10.1016/j.ijthermalsci.2015.01.026.

[28] Kazumi Matsui, Kenjiro Terada, and Kohei Yuge. Two-scale finite element analysis of heterogeneous solids with periodic microstructures. *Computers & Structures*, 82(7-8):593–606, 2004. doi:10.1016/j.compstruc.2004.01.004.

[29] Christian Miehe, Jörg Schröder, and Martin Becker. Computational homogenization analysis in finite elasticity: material and structural instabilities on the micro- and macro-scales of periodic composites and their interaction. *Computer Methods in Applied Mechanics and Engineering*, 191(44):4971–5005, 2002. doi:10.1016/s0045-7825(02)00391-2.

[30] David Modesto, Sergio Zlotnik, and Antonio Huerta. Proper generalized decomposition for parameterized Helmholtz problems in heterogeneous and unbounded domains: Application to harbor agitation. *Computer Methods in Applied Mechanics and Engineering*, 295:127–149, oct 2015. doi:10.1016/j.cma.2015.03.026.

[31] E. Monteiro, J. Yvonnet, and Q. C. He. Computational homogenization for nonlinear conduction in heterogeneous materials using model reduction. *Computational Materials Science*, 42(4):704–712, jun 2008. doi:10.1016/j.commatsci.2007.11.001.

[32] J. Oliver, M. Caicedo, A. E. Huespe, J. A. Hernández, and E. Roubin. Reduced order modeling strategies for computational multiscale fracture. *Computer Methods in Applied Mechanics and Engineering*, 313:560–595, jan 2017. doi:10.1016/j.cma.2016.09.039.

[33] I. Özdemir, W. A. M. Brekelmans, and M. G. D. Geers. Computational homogenization for heat conduction in heterogeneous solids. *International Journal for Numerical Methods in Engineering*, 73(2):185–204, 2007. doi:10.1002/nme.2068.

[34] I. Özdemir, W. A. M. Brekelmans, and M. G. D. Geers. FE2 computational homogenization for the thermo-mechanical analysis of heterogeneous solids. *Computer Methods in Applied Mechanics and Engineering*, 198(3-4):602–613, dec 2008. doi:10.1016/j.cma.2008.09.008.

[35] René Pinnau. Model reduction via proper orthogonal decomposition. In Wilhelmus H. A. Schilders, Henk A. van der Vorst, and Joost Rommes, editors, *Model Order Reduction: Theory, Research Aspects and Applications*, pages 95–109. Springer Berlin Heidelberg, Berlin, Heidelberg, 2008. doi:10.1007/978-3-540-78841-6_5.

[36] A. Radermacher and S. Reese. POD-based model reduction with empirical interpolation applied to nonlinear elasticity. *International Journal for Numerical Methods in Engineering*, 107(6):477–495, dec 2015. doi:10.1002/nme.5177.

[37] D. Ryckelynck. Hyper-reduction of mechanical models involving internal variables. *International Journal for Numerical Methods in Engineering*, 77(1):75–89, jan 2009. doi:10.1002/nme.2406.

[38] E. Sanchez-Palencia. Non-homogeneous media and vibration theory. volume 127 of *Lecture Notes in Physics*. Springer Berlin Heidelberg, 1980. doi:10.1007/3-540-10000-8.

[39] Roland Schobi, Bruno Sudret, and Joe Wiart. Polynomial-chaos-based Kriging. *International Journal for Uncertainty Quantification*, 5(2):171–193, 2015. doi:10.1615/int.j.uncertaintyquantification.2015012467.

[40] P. M. Suquet. *Plasticité et homogénéisation*. PhD thesis, Université Pierre et Marie Curie, Paris 6, 1982.

[41] K. Terada and N. Kikuchi. A class of general algorithms for multi-scale analyses of heterogeneous media. *Computer Methods in Applied Mechanics and Engineering*, 190(40-41):5427–5464, 2001. doi:10.1016/s0045-7825(01)00179-7.

[42] Giorgio Tomasi and Rasmus Bro. PARAFAC and missing values. *Chemometrics and Intelligent Laboratory Systems*, 75(2):163–180, feb 2005. doi:10.1016/j.chemolab.2004.07.003.

[43] Yangyang Xu. Fast algorithms for higher-order singular value decomposition from incomplete data. *Journal of Computational Mathematics*, 35(4):397–422, jun 2017. doi:10.4208/jcm.1608-m2016-0641.

[44] Y. Yang, F. Y. Ma, C. H. Lei, Y. Y. Liu, and J. Y. Li. Nonlinear asymptotic homogenization and the effective behavior of layered thermoelectric composites. *Journal of the Mechanics and Physics of Solids*, 61(8):1768–1783, 2013. doi:10.1016/j.jmps.2013.03.006.

[45] J. Yvonnet and Q.-C. He. The reduced model multiscale method (R3M) for the non-linear homogenization of hyperelastic media at finite strains. *Journal of Computational Physics*, 223(1):341–368, April 2007. doi:10.1016/j.jcp.2006.09.019.

[46] H. W. Zhang, S. Zhang, J. Y. Bi, and B. A. Schrefler. Thermo-mechanical analysis of periodic multiphase materials by a multiscale asymptotic homogenization approach. *International Journal for Numerical Methods in Engineering*, 69(1):87–113, 2006. doi:10.1002/nme.1757.

[47] Yang Zi-Hao, Chen Yun, Yang Zhi-Qiang, and Ma Qiang. Dynamic thermo-mechanical coupled response of random particulate composites: A statistical two-scale method. *Chinese Physics B*, 23(7):076501, jul 2014. doi:10.1088/1674-1056/23/7/076501.